Divinylphenylene-Bridged Diruthenium Complexes Bearing $Ru(CO)Cl(P^iPr_3)_2$ Entities†

Jörg Maurer,[‡,§] Biprajit Sarkar,[§] Brigitte Schwederski,[§] Wolfgang Kaim,[§] Rainer F. Winter,*[,‡] and Stanislav Záliš[||]

Institut für Anorganische Chemie der Universität Regensburg, Universitätsstrasse 31, D-93040 Regensburg, Germany, Institut für Anorganische Chemie der Universität Stuttgart, Pfaffenwaldring 55, D-70569 Stuttgart, Germany, and J. Heyrovský Institute of Physical Chemistry, Academy of Sciences of the Czech Republic, Dolejškova 3, Prague, Czech Republic

Received March 24, 2006

The divinylphenylene-bridged diruthenium complexes (*E,E*)-[{$(P^iPr_3)_2(CO)ClRu$}$_2$(μ-HC═CHC_6H_4CH═CH-1,3)] (**m-2**) and (*E,E*)-[{$(P^iPr_3)_2(CO)ClRu$}$_2$(μ-HC═CHC_6H_4CH═CH-1,4)] (**p-2**) have been prepared and compared to their PPh_3-containing analogues **m-1** and **p-1**. The higher electron density at the metal atoms increases the contribution of the metal end groups to the bridge-dominated occupied frontier orbitals and stabilizes the various oxidized forms with respect to those of **m-1** and **p-1**. This has been confirmed and quantified electrochemically, because the two reversible oxidation waves were observed at considerably lower potentials than for the PPh_3 complexes. Owing to their greater stability, the one- and two-electron-oxidized forms **m-2**$^{n+}$ and **p-2**$^{n+}$ of both complexes could be generated and spectroscopically characterized inside an optically transparent thin layer electrolysis cell. UV/vis/near-IR and ESR spectroelectrochemistry indicates that the oxidation processes are centered at the organic bridging ligand. σ-Bonded divinylphenylenes thus constitute an unusual class of "noninnocent" ligands for organometallic compounds. Electronic transitions observed for the mono- and dioxidized forms closely resemble those of donor-substituted phenylenevinylene compounds, including oligo(phenylenevinylenes) (OPVs) and poly(phenylenevinylene) (PPV) in the respective oxidation states. Strong ESR signals and nearly isotropic **g** tensors are observed for the monocations in fluid and frozen solutions. The metal contribution to the redox orbitals is illustrated by a shift of the CO stretching bands to notably higher energies upon stepwise oxidation. The shifts strongly exceed those observed for the PPh_3 containing, six-coordinated species (*E,E*)-[{$(PPh_3)_2(CO)Cl(L)Ru$}$_2$(μ-HC═CHC_6H_4CH═CH)]$^{n+}$ (L = substituted pyridine). IR spectroelectrochemistry reveals the presence of two electronically different transition-metal moieties in **m-2**$^+$, while they resemble each other more closely in **p-2**$^+$. Differences in electronic coupling are illustrated by the charge distribution parameters calculated from the spectra. Bulk electrolysis experiments confirm the results from the in situ spectroelectrochemistry and the overall stoichiometry of the redox processes. Quantum-chemical calculations were performed in order to provide insight into the nature and composition of the frontier orbitals. The electronic transitions observed for the neutral forms were assigned by TD DFT. IR frequencies calculated for **m-2** and **p-2** in their various oxidation states retrace the experimental observations. They fail, however, in the case of **m-2**$^+$, where a symmetrical structure is calculated, as opposed to the distinctly asymmetric electron distribution observed by IR spectroscopy. Geometry-optimized structures were calculated for all accessible oxidation states. The structural changes following stepwise oxidation agree well with the experimental findings: e.g., a successive low-energy shift of the C═C stretching vibration of the bridge. The radical cation **m-2**$^+$ displays a broad composite electronic absorption band at low energy that extends into the mid-IR region.

Introduction

Complexes in which two redox-active transition-metal moieties are linked together by an unsaturated conjugated bridging ligand have received great interest, first as a testing ground for all aspects related to intramolecular electron transfer and then as models for and principal constituents of possibly conducting molecule-based "wires". In adhering to this picture, the redox-active end groups are mostly viewed as the voltage source or drain, while the bridge serves as the conduit. The voltage gradient is then established by oxidizing or reducing one of the terminal redox sites, thus generating a mixed-valent state.[1] Here it is possible to probe the degree of electron delocalization and the rate at which the odd electron and the charge generated during the redox process are transmitted between the end groups. This can be done by analyzing ESR hyperfine splitting involving active nuclei in the bridge or at the metal centers, by investigating the redox-induced changes in the shifts and band patterns of charge-sensitive infrared- or Raman-active functions which accompany electron transfer in vibrational spectroscopy, or by analyzing the typical intervalence charge transfer (IVCT) bands

* To whom correspondence should be addressed. E-mail: rainer.winter@chemie.uni-regensburg.de. Fax: +49 941 9434488.

† Dedicated to Prof. Piero Zanello on the occasion of his 65th birthday.

‡ Universität Regensburg.

§ Universität Stuttgart.

|| Academy of Sciences of the Czech Republic.

(1) Launay, J.-P. *Chem. Soc. Rev.* **2001**, *30*, 386.

10.1021/om0602660 CCC: $33.50
Publication on Web 06/16/2006

which often appear in the low-energy end of the visible region or the near-IR region.

Highly unsaturated hydrocarbon bridges offer an extended π-system and have been recognized as particularly effective coupling units. A vast number of oligoynediyl- and diethynylarylene-bridged dimetal complexes have thus been synthesized and investigated.[2−24] Oligoenediyl bridges, though less well precedented, are also efficient electronic coupling units with sometimes even better performances than their oligoynediyl counterparts.[25,26] Efficient electronic coupling usually requires that the unsaturated bridge contribute to the singly occupied MO (SOMO). The bridge thus constitutes an integral part of the entire redox system. C_4-bridged dimetal complexes provide particularly instructive examples, and redox-induced interconversions between dimetal butadiynediyl and butatrienylidene or between butatrienylidene and ethynylbis(carbyne) binding motifs are known, depending on the electron count of the metal.[2,3,5,7,20,22,27−32] However, despite large contributions of the bridge, the redox processes in these systems are clearly dominated by the metal.

We have recently observed that the divinylphenylene-bridged diruthenium complex (*E*,*E*)-[{$(PPh_3)_2$(CO)Cl(4-EtOOCpy)Ru}$_2$-(μ-HC═CHC_6H_4CH═CH-1,3)] and its mononuclear styryl derivative constitute examples where the redox processes are dominated by the unsaturated organic ligand. Further investigations have shown that this holds irrespective of the complexes' topology: i.e., for both the 1,3- and the 1,4-isomers.[33] As a consequence of the largely ligand-centered oxidations, none of these complexes exhibited any IVCT band in its monooxidized, formally mixed-valent state. Quantum-chemical calculations suggest that the occupied frontier orbitals correspond to antibonding interactions between higher lying, nearly degenerate π levels of the bridge and lower lying metal d_π orbitals. It thus seemed logical to increase the energies of the d energy levels of the metal in order to seek for a more balanced electron distribution within these systems. We herein show that changing the {$Ru(PPh_3)_2L$} moieties to {$Ru(P^iPr_3)_2$} induces a higher metal character of the frontier orbitals. The $Ru(P^iPr_3)_2$(CO)Cl group stabilizes the oxidized forms to such a degree that even the dications could be conveniently studied by vibrational and electronic spectroscopy.

Experimental Section

All manipulations were performed by standard Schlenk techniques under an argon atmosphere. Solvents were dried by standard procedures and degassed by saturation with argon prior to use. Ether employed in the washing process was saturated with argon but otherwise used as received. Infrared spectra were obtained on a Perkin-Elmer Paragon 1000 PC FT-IR instrument. ^{1}H (250.13 MHz), ^{13}C (62.90 MHz), and ^{31}P NMR spectra (101.26 MHz) were recorded on a Bruker AC 250 spectrometer as $CDCl_3$ solutions at 303 K or in the solvent indicated. The spectra were referenced to the residual protonated solvent (^{1}H), the solvent signal itself (^{13}C), or external H_3PO_4 (^{31}P). If necessary, the assignment of ^{13}C NMR spectra was aided by DEPT-135 experiments. UV/vis spectra were obtained on an Omega 10 spectrometer from Bruins Instruments in HELMA quartz cuvettes whith 1 cm optical path lengths or on a J&M TIDAS diode array spectrometer. The ESR equipment consisted of a Bruker ESP 3000 spectrometer equipped with an HP 5350 B frequency counter, a Bruker ER 035 M NMR gaussmeter, and an ESR 900 continuous flow cryostat from Oxford Instruments for low-temperature work. Elemental analyses (C, H, N) were performed at in-house facilities. The equipment for voltammetric and spectroelectrochemical studies and the conditions employed in this work were as described elsewhere.[34] The cell used in quantitative coulometry experiments was a home-built three compartment H-cell with a 3.5 cm diameter Pt/Ir alloy basket as the working electrode and a smaller 1 cm diameter basket as the counter electrode. A silver plate was used as the reference electrode. The electrodes are welded to platinum wires (Supratronic), and the platinum wires are welded to wires manufactured of Vakon alloy; these in turn were sealed into 10 mm diameter glass tubes. The electrodes were inserted into the cell via standard joints and fixed by using Quickfit seals. The cell can be attached to a Schlenk line through a joint attached to the central working electrode compartment and charged via inlets on top of each compartment. Individual compartments are separated via medium-porosity frits.

Molecular Orbital Calculations. Quantum-chemical studies were performed without any symmetry constraints on PMe_3-

(2) Bruce, M. I.; Low, P. J.; Costuas, K.; Halet, J.-F.; Best, S. P.; Heath, G. A. *J. Am. Chem. Soc.* **2000**, *122*, 1949.
(3) Bruce, M. I.; Ellis, B. G.; Low, P. J.; Skelton, B. W.; White, A. H. *Organometallics* **2003**, *22*, 3184.
(4) Bruce, M. I.; Kostuas, K.; Davin, T.; Ellis, B. G.; Halet, J.-F.; Lapinte, C.; Low, P. J.; Smith, M. E.; Skelton, B. W.; Toupet, L.; White, A. H. *Organometallics* **2005**, *24*, 3864.
(5) Le Narvor, N.; Toupet, L.; Lapinte, C. *J. Am. Chem. Soc.* **1995**, *117*, 7129.
(6) Coat, F.; Guillevic, M.-A.; Toupet, L.; Paul, F.; Lapinte, C. *Organometallics* **1997**, *16*, 5988.
(7) Guillemot, M.; Toupet, L.; Lapinte, C. *Organometallics* **1998**, *17*, 1928.
(8) Paul, F.; Meyer, W. E.; Toupet, L.; Jiao, H.; Gladysz, J. A.; Lapinte, C. *J. Am. Chem. Soc.* **2000**, *122*, 9405.
(9) Paul, F.; Costuas, K.; Ledoux, I.; Deveau, S.; Zyss, J.; Halet, J.-F.; Lapinte, C. *Organometallics* **2002**, *21*, 5229.
(10) Coat, F.; Paul, F.; Lapinte, C.; Toupet, L.; Costuas, K.; Halet, J.-F. *J. Organomet. Chem.* **2003**, *683*, 368.
(11) Jiao, H.; Costuas, K.; Gladysz, J. A.; Halet, J.-F.; Guillemot, M.; Toupet, L.; Paul, F.; Lapinte, C. *J. Am. Chem. Soc.* **2003**, *125*, 9511.
(12) Weyland, T.; Lapinte, C.; Frapper, G.; Calhorda, M. J.; Halet, J.-F.; Toupet, L. *Organometallics* **1997**, *16*, 2024.
(13) Weyland, T.; Costuas, K.; Mari, A.; Halet, J.-F.; Lapinte, C. *Organometallics* **1998**, *17*, 5569.
(14) Weyland, T.; Costuas, K.; Toupet, L.; Halet, J.-F.; Lapinte, C. *Organometallics* **2000**, *19*, 4228.
(15) Le Stang, S.; Paul, F.; Lapinte, C. *Organometallics* **2000**, *19*, 1035.
(16) Roué, S.; Lapinte, C. *J. Organomet. Chem.* **2005**, *690*, 594.
(17) de Montigny, F.; Argouarch, G.; Costuas, K.; Halet, J.-F.; Roisnel, T.; Toupet, L.; Lapinte, C. *Organometallics* **2005**, *24*, 4558.
(18) Dembinski, R.; Bartik, T.; Bartik, B.; Jaeger, M.; Gladysz, J. A. *J. Am. Chem. Soc.* **2000**, *122*, 810.
(19) Szafert, S.; Gladysz, J. A. *Chem. Rev.* **2003**, *103*, 4175.
(20) Kheradmandan, S.; Heinze, K.; Schmalle, H. W.; Berke, H. *Angew. Chem.* **1999**, *111*, 2412.
(21) Venkatesan, K.; Fernández, F. J.; Blacque, O.; Fox, T.; Alfonso, M.; Schmalle, H. W.; Berke, H. *Chem. Commun.* **2003**, 2006.
(22) Fernández, F. J.; Venkatesan, K.; Blacque, O.; Alfonso, M.; Schmalle, H. W.; Berke, H. *Chem. Eur. J.* **2003**, *9*, 6192.
(23) Kheradmandan, S.; Venkatesan, K.; Blacque, O.; Schmalle, H. W.; Berke, H. *Chem. Eur. J.* **2004**, *10*, 4872.
(24) Venkatesan, K.; Fox, T.; Schmalle, H. W.; Berke, H. *Organometallics* **2005**, *24*, 2834.
(25) Sponsler, M. B. *Organometallics* **1995**, *14*, 1920.
(26) Chung, M.-C.; Gu, X.; Etzenhouser, B. A.; Spuches, A. M.; Rye, P. T.; Seetharaman, S. K.; Rose, D. J.; Zubieta, J.; Sponsler, M. B. *Organometallics* **2003**, *22*, 3485.
(27) Fernández, F. J.; Blacque, O.; Alfonso, M.; Berke, H. *Chem. Commun.* **2001**, 1266.
(28) Zhou, Y.; Seyler, J. W.; Weng, W.; Arif, A. M.; Gladysz, J. A. *J. Am. Chem. Soc.* **1993**, *115*, 8509.
(29) Brady, M.; Weng, W.; Zhou, Y.; Seyler, J. W.; Amoroso, A. J.; Arif, A. M.; Böhme, M.; Frenking, G.; Gladysz, J. A. *J. Am. Chem. Soc.* **1997**, *119*, 775.
(30) Woodworth, B. E.; White, P. S.; Templeton, J. L. *J. Am. Chem. Soc.* **1997**, *119*, 828.
(31) Le Narvor, N.; Lapinte, C. *J. Chem. Soc., Chem. Commun.* **1993**, 357.
(32) Coat, F.; Lapinte, C. *Organometallics* **1996**, *15*, 477.
(33) Maurer, J.; Winter, R.; Sarkar, B. Manuscript in preparation.
(34) Winter, R. F.; Klinkhammer, K.-W.; Zális, S. *Organometallics* **2001**, *20*, 1317.

substituted models **m-2**$^{\mathbf{Me}\,n+}$ and **p-2**$^{\mathbf{Me}\,n+}$ ($n = 0-2$) instead of the P^iPr_3 complexes. The ground-state electronic structure was calculated by density functional theory (DFT) methods using the ADF2005.01[35,36] and Gaussian 03[37] program packages. Within ADF, Slater type orbital (STO) basis sets of triple-ζ quality with polarization functions were employed, with the exception of the CH_3 substituents on the P atoms, which were described by using a double-ζ basis. The inner shells were represented by a frozen-core approximation: i.e., 1s for C and N, 1s−2p for P and Cl, and 1s−3d for Ru were kept frozen. The calculations were done with a functional including Becke's gradient correction[38] to the local exchange expression in conjunction with Perdew's gradient correction[39] to the local correlation (ADF/BP). The following density functionals were used within ADF: a local density approximation (LDA) with VWN parametrization of electron gas data and a functional including Becke's gradient correction[38] to the local exchange expression in conjunction with Perdew's gradient correction[39] to the LDA expression (ADF/BP). The scalar relativistic (SR) zero-order regular approximation (ZORA)[40] was used within this study. The **g** tensor was obtained from a spin-nonpolarized wave function after incorporating the spin−orbit (SO) coupling by first-order perturbation theory from the ZORA Hamiltonian in the presence of a time-independent magnetic field.[41,42]

Within G03 calculations the quasirelativistic effective core pseudopotentials and the corresponding optimized set of basis functions for Ru[43] and 6-31G* polarized double-ζ basis sets[44] for the remaining atoms were employed together with the B3LYP[45] or BPW91[38] functional.

Synthesis of [{Ru(P^{i}Pr$_3$)$_2$(CO)Cl}$_2$(μ-CH=CHC$_6$H$_4$CH=CH-1,3)] (m-2). To a stirred solution of [RuHCl(CO)(P^{i}Pr$_3$)$_2$] (0.27 g, 0.555 mmol) in CH_2Cl_2 (10 mL) was slowly added a solution of 1,3-diethynylbenzene (0.035 g, 0.277 mmol) in CH_2Cl_2 (10 mL). After the reaction mixture was stirred for 30 min, the solvent was removed under reduced pressure. The red product was washed twice with *n*-hexane, filtered off, and dried under vacuum. Yield: 195 mg (64%). Anal. Calcd (found): C, 52.5 (51.31); H, 8.44 (8.47). ^{1}H NMR (200 MHz, $CDCl_3$, 293 K): δ 8.43 (dt, 2H, $^3J_{H-H} = 13.27$ Hz, $^4J_{P-H} = 0.8$ Hz, RuC=CH), 7.24 (s, 1H, phenyl (bridge)), 6.98 (t, 1H, $^3J_{H-H} = 7.75$ Hz, phenyl (bridge)), 6.68 (virtual t, 2H, $J_{H-H} = 6.63$ Hz, phenyl (bridge)), 5.89 (dt, 2H, $^3J_{H-H} = 13.27$ Hz, $^3J_{P-H} = 1.9$ Hz, RuHC=C), 2.83−2.26 (m, 12H, P^{i}Pr$_3$), 1.52−1.16 (m, 72H, P^{i}Pr$_3$). ^{31}P NMR (80 MHz, $CDCl_3$, 20 °C): δ 38.4 (s). IR (KBr, ν in cm^{-1}): 1910 (CO), 1555, 1470 (C=C, aryl, vinyl).

Chart 1

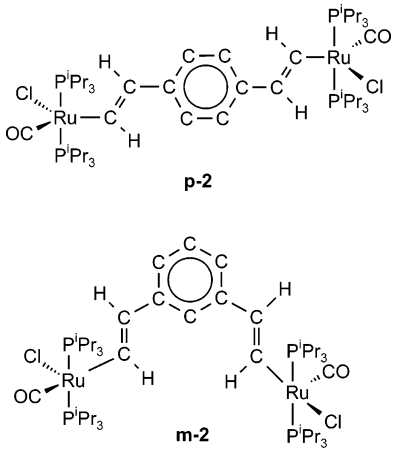

Synthesis of [{Ru(P^{i}Pr$_3$)$_2$(CO)Cl}$_2$(μ-CH=CHC$_6$H$_4$CH=CH-1,4)] (p-2). A solution of 1,4-diethynylbenzene (0,029 g, 0.299 mmol) in CH_2Cl_2 (10 mL) was slowly added to a stirred solution of [RuHCl(CO)(P^{i}Pr$_3$)$_2$] (0.212 g, 0.435 mmol) in CH_2Cl_2 (10 mL). The reaction mixture was stirred for 30 min. The solvent was evaporated under reduced pressure, and the red product was washed twice with *n*-hexane, filtered off, and dried under vacuum. Yield: 0.166 g (66%). Anal. Calcd (found): C, 52.50 (52.45); H, 8.44 (8.19). ^{1}H NMR (250 MHz, $CDCl_3$, 20 °C): δ 8.27 (dt, 2H, $^3J_{H-H} = 13.2$ Hz, $^4J_{H-P} = 0.7$ Hz, RuC=CH), 6.82 (virtual t, 2H, $^4J_{H-H} = 6.6$ Hz, phenyl (bridge)), 5.87 (dt, 2H, $^3J_{H-H} = 13.16$ Hz, $^3J_{H-P} = 2.4$ Hz, RuHC=C), 2.84−2.60 (m, 12H, P^{i}Pr$_3$), 1.39−1.15 (m, 72H, P^{i}Pr$_3$). ^{31}P NMR (100 MHz, $CDCl_3$, 20 °C): δ 38.2 (s). IR (KBr, ν in cm^{-1}): 1910 (CO), 1565, 1450 (C=C aryl, vinyl).

Results and Discussion

Synthesis and Characterization. The dinuclear divinylphenylene-bridged complex {(P^{i}Pr$_3$)$_2$(CO)ClRu}(μ-CH=CHC$_6$H$_4$HC=CH-1,3) (**m-2**) and its 1,4-isomer **p-2** (see Chart 1) were readily prepared by reacting the hydride HRu(CO)Cl(P^{i}Pr$_3$)$_2$ with the corresponding diethynylbenzene in CH_2Cl_2 in a stoichiometric ratio of slightly larger than 2:1. Upon addition of the alkyne the dark yellow solution of the hydride rapidly turned red, indicating formation of the vinyl complexes, and the reactions were complete within a few minutes. This short time is despite the rather intricate reaction mechanism, which, according to experimental and quantum-chemical studies conducted for the osmium analogue, includes adduct formation and the nonproductive formation of vinylidene complexes.[46] The pure products were obtained as intense red microcrystalline solids by evaporating the solvent and washing the residue with cold hexane to remove small quantities of excess hydride. Product identity was confirmed by ^{31}P NMR spectroscopy and the characteristic NMR resonance signals of the vinyl protons. These gave well-resolved doublet-of-triplet patterns with a large $^3J_{HH}$ coupling constant of around 13 Hz, indicating formal cis addition of the Ru−H bond to the alkyne and smaller ^3J and ^4J couplings to the phosphine P atoms. Unlike their PPh_3-substituted counterparts, complexes **2**, despite being coordina-

(35) te Velde, G.; Bickelhaupt, F. M.; van Gisbergen, S. J. A.; Fonseca Guerra, C.; Baerends, E. J.; Snijders, J. G.; Ziegler, T. *J. Comput. Chem.* **2001**, *22*, 931.

(36) SCM, T. C. ADF2005.01; Vrije Universiteit, Amsterdam, Amsterdam, The Netherlands, 2005.

(37) Frisch, M. J.; Trucks, G. W.; Schlegel, H. B.; Scuseria, G. E.; Robb, M. A.; Cheeseman, J. R.; Montgomery, J. A., Jr.; Vreven, T.; Kudin, K. N.; Burant, J. C.; Millam, J. M.; Iyengar, S. S.; Tomasi, J.; Barone, V.; Mennucci, B.; Cossi, M.; Scalmani, G.; Rega, N.; Petersson, G. A.; Nakatsuji, H.; Hada, M.; Ehara, M.; Toyota, K.; Fukuda, R.; Hasegawa, J.; Ishida, M.; Nakajima, T.; Honda, Y.; Kitao, O.; Nakai, H.; Klene, M.; Li, X.; Knox, J. E.; Hratchian, H. P.; Cross, J. B.; Bakken, V.; Adamo, C.; Jaramillo, J.; Gomperts, R.; Stratmann, R. E.; Yazyev, O.; Austin, A. J.; Cammi, R.; Pomelli, C.; Ochterski, J. W.; Ayala, P. Y.; Morokuma, K.; Voth, G. A.; Salvador, P.; Dannenberg, J. J.; Zakrzewski, V. G.; Dapprich, S.; Daniels, A. D.; Strain, M. C.; Farkas, O.; Malick, D. K.; Rabuck, A. D.; Raghavachari, K.; Foresman, J. B.; Ortiz, J. V.; Cui, Q.; Baboul, A. G.; Clifford, S.; Cioslowski, J.; Stefanov, B. B.; Liu, G.; Liashenko, A.; Piskorz, P.; Komaromi, I.; Martin, R. L.; Fox, D. J.; Keith, T.; Al-Laham, M. A.; Peng, C. Y.; Nanayakkara, A.; Challacombe, M.; Gill, P. M. W.; Johnson, B.; Chen, W.; Wong, M. W.; Gonzalez, C.; Pople, J. A. *Gaussian 03*, revision B.2; Gaussian, Inc.: Wallingford, CT, 2004.

(38) Becke, A. D. *Phys. Rev. A* **1988**, *38*, 3098.

(39) Perdew, J. P. *Phys. Rev. A* **1986**, *33*, 8822.

(40) van Lenthe, E.; Ehlers, A. E.; Baerends, E. J. *J. Chem. Phys.* **1999**, *110*, 8943.

(41) van Lenthe, E.; van der Avoird, A.; Wormer, P. E. S. *J. Chem. Phys.* **1997**, *107*, 2488.

(42) van Lenthe, E.; van der Avoird, A.; Wormer, P. E. S. *J. Chem. Phys.* **1998**, *108*, 4783.

(43) Andrae, D.; Haeussermann, U.; Dolg, M.; Stoll, H.; Preuss, H. *Theor. Chim. Acta* **1990**, *77*, 123.

(44) Hariharan, P. H.; Pople, J. A. *Theor. Chim. Acta* **1973**, *28*, 213.

(45) Stephens, P. J.; Devlin, F. J.; Cabalowski, C. F.; Frisch, M. J. *J. Phys. Chem.* **1994**, *98*, 11623.

(46) Marchenko, A. V.; Gérard, H.; Eisenstein, O.; Caulton, K. G. *New J. Chem.* **2001**, *25*, 1244.

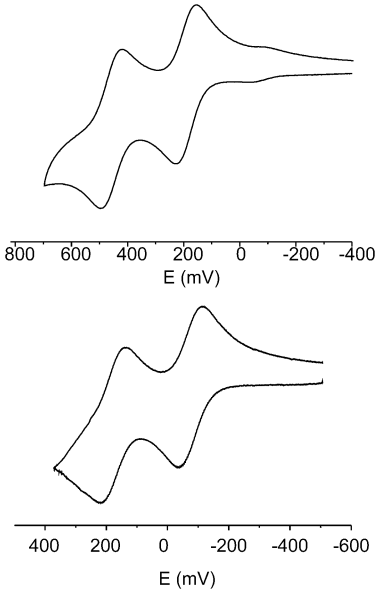

Figure 1. Cyclic voltammograms of **m-2** (upper curve) and **p-2** (lower curve) at room temperature in CH_2Cl_2/0.2 M NBu_4PF_6 (υ = 0.1 V/s). Potentials are calibrated against the ferrocene/ferrocenium standard.

Table 1. Redox Properties of the Five-Coordinate Complexes $\{(PR_3)_2Ru(CO)Cl\}_nL$

compd	$E_{1/2}{}^{0/+}$, V	$E_{1/2}{}^{+/2+}$, V	$\Delta E_{1/2}$, mV
m-2	0.190	0.460	270
p-2	−0.075	0.175	250
m-1	0.310[a]	0.490[a]	180
p-1	0.180[a,b]		

[a] Half-wave potentials of chemically partially reversible processes at −78 °C. [b] Composite wave.

tively unsaturated, have only little propensity toward the addition of a sixth ligand. This is certainly due to the superior donor properties of the P^iPr_3 ligand as compared to those of PPh_3 and to the steric crowding. Higher electron density at the ruthenium despite coordinative unsaturation is evident from the position of the CO stretching band in the IR spectra. That band appears at ca. 1910 cm^{-1} for complexes **m-2** and **p-2**, ca. 15−20 cm^{-1} lower than for the six-coordinated bis(triphenylphosphine) 4-picoline or bis(triphenylphosphine) 4-isonicotinate congeners.[33]

Electrochemistry. In CH_2Cl_2/TBAPF$_6$ **m-2** and **p-2** undergo two consecutive, chemically and electrochemically reversible one-electron-oxidation processes (Figure 1, Table 1). This is in stark contrast to the case for five-coordinated PPh_3-containing analogues, which give irreversible responses at ambient temperature and only limited chemical reversibility as the temperature is lowered to 195 K. Likewise, the half-wave potentials of **m-2** and **p-2** are shifted by 120 and 255 mV, respectively, toward more negative (cathodic) potentials in comparison to the half-wave potentials (195 K) of the PPh_3-substituted species. The half-wave potentials of **m-2** and **p-2** are even somewhat lower than those of coordinatively saturated pyridine adducts with PPh_3 ligands.[47] Considering that the oxidation processes mainly involve the bridging ligand (vide infra), the redox potentials are, however, only an indirect probe of the electron densities at the metal atoms; rather, they track the electron-releasing properties of the $\{RuL_2(CO)Cl\}$ entities toward the divinylphenylene ligands.

For complexes of the general architecture {M}−bridge−{M} with redox-active transition-metal-based end groups {M}, the differences in half-wave potentials $E_{1/2}$, $\Delta E_{1/2}$, are usually considered as reflecting a kind of electronic interaction (or communication) between the remote redox sites, with larger splittings as the intermetal interactions increase. The closely related isomeric diethynylphenylene-bridged diruthenium complexes $\{Cl(dppm)_2Ru\}_2(\mu$-C≡CC_6H_4-C≡C-1,3 or -1,4) display $\Delta E_{1/2}$ values of 190 and 300 mV, respectively.[48] Further instructive examples of such behavior are known from diethynylphenylene-bridged dinuclear complexes of iron[12,49] and osmium.[48] π-Conjugation is much more efficient for the para isomer, and the potential splitting for the latter is hence substantially larger than that for the meta form. A mutual relation between differences in $E_{1/2}$ and the degree of the electronic interaction between the metal sites has been corroborated by the determination of electronic coupling, as provided by the position and the shape of the intervalence charge transfer (IVCT) bands in the near-IR region (vide infra).[12,48]

Electrochemistry makes the different characteristics of the divinylphenylene-bridged complexes, as opposed to the bis(ethynyl)phenylene-bridged counterparts, immediately apparent. In the former, the $\Delta E_{1/2}$ value of the meta isomer slightly exceeds that of the para isomer (270 vs 250 mV). This counterintuitive result shows that a metal-based description as above does not apply to the divinylphenylene systems presented here. In complexes such as **m-2** and **p-2**, the occupied frontier levels (redox orbitals) are dominated by the unsaturated ligands.[47] In this respect, it is quite revealing to compare the voltammetric responses of complexes **2** to those of purely organic phenylenevinylene compounds. Under the appropriate conditions, the latter are oxidized in sequential one-electron steps with potential separations of ca. 90−180 mV that resemble those observed for complexes **2**. Oxidation potentials are lowered as the number of phenylenevinylene repeat units increases or as donor substituents are added.[50−52] The redox potentials of even heavily donor substituted phenylenevinylenes are, however, substantially more anodic (>0.6 V vs Fc/Fc^+) than those observed for complexes **2**. When they are viewed in this manner, the $\{Ru(PR_3)_2(CO)Cl(L)\}$ entities act as powerful electron-donor substituents that even surpass common organic donor substituents such as dimethylamino or alkoxy groups. This view also agrees with the finding that the oxidation potentials of **p-2**, where the $\{(P^iPr_3)_2(CO)ClRu\}$ moieties are in direct conjugation with the divinylphenylene ligand, are distinctly lower than for **m-2**, where such conjugation is expected to be less efficient. The metal entities probably have higher contributions to the redox orbitals than more conventional organic donor substituents. The site of attachment, i.e., the vinyl rather than the phenyl groups, may also play a role.

UV/Vis/Near-IR Spectroelectrochemistry. Verification of bridge-dominated oxidation in the divinylphenylene-bridged dinuclear complexes stems from the changes in their electronic spectra upon oxidation. For metal-centered oxidation processes one expects a lowering of the intensities of metal-to-ligand

(47) Maurer, J.; Winter, R. F.; Sarkar, B.; Fiedler, J.; Záliš, S. *Chem. Commun.* **2004**, 1900.

(48) Colbert, M. C. B.; Lewis, J.; Long, N. J.; Raithby, P. R.; Younus, M.; White, A. J. P.; Williams, D. J.; Payne, N. N.; Yellowlees, L.; Beljonne, D.; Chawdhury, N.; Friend, R. H. *Organometallics* **1998**, *17*, 3034.

(49) Le Narvor, N.; Lapinte, C. *Organometallics* **1995**, *14*, 634.

(50) Klärner, G.; Former, C.; Yan, X.; Richert, R.; Müllen, K. *Adv. Mater.* **1996**, *8*, 932.

(51) Heinze, J.; Mortensen, J.; Müllen, K.; Schenk, R. *J. Chem. Soc., Chem. Commun.* **1987**, 701.

(52) Ndayikengurukiye, H.; Jacobs, S.; Tachelet, W.; Van der Looy, J.; Pollaris, A.; Geise, H. J.; Claeys, M.; Kauffmann, J. M.; Janietz, S. *Tetrahedron* **1997**, *53*, 13811.

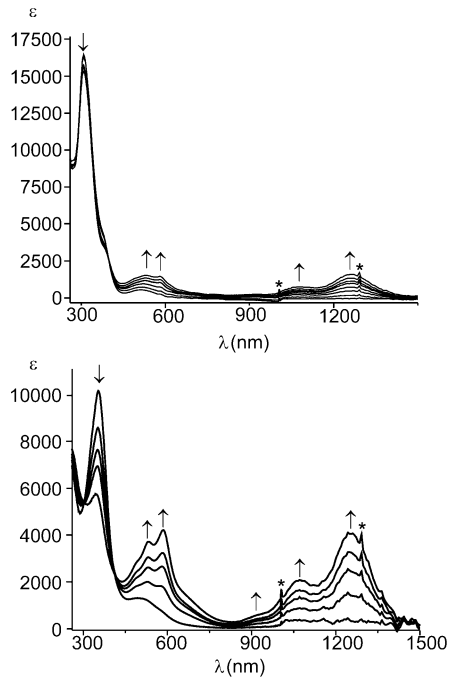

Figure 2. UV/Vis/near-IR spectra recorded during the first oxidations of **m-2** (upper graph) and **p-2** (lower graph). Spikes marked by asterisks denote instrumental artifacts.

charge transfer (MLCT) bands and the appearance of new absorptions corresponding to the transfer of charge from any donor ligand(s) to the now electron-deficient metal center (LMCT). If, however, the oxidation involves the bridging ligand, any new absorption generated in the oxidation process should be more of a $\pi \rightarrow \pi^*$ parentage and closely resemble the absorptions observed for similar, purely organic congeners. This is indeed the case here as follows from UV/vis/near-IR spectroelectrochemistry (see Figure 2). The orange-red color of the neutral starting compounds arises from transitions at 492 (**p-2**) or 513 nm (**m-2**) that involve an excitation mainly from the bridging ligand to orbitals that are delocalized over the metal and the phosphine ligands and are thus assigned as mixed LLCT/LMCT transitions (vide infra). Upon sequential oxidation inside an optically transparent thin layer electrolysis (OTTLE) cell,[53] this band is gradually replaced by a structured, more intense feature with the main peak at a slightly higher energy (see Figure 2). Another band with easily discernible vibrational progression grows in at ca. 1260 nm (see footnotes *b* and *e* of Table 2). In both cases there are two isosbestic points for the conversions of the neutral to the monocationic forms at 302 and 414 nm for **p-2** and at 295 and 398 nm for the oxidation of the meta isomer **m-2**. While the overall spectral patterns are very similar, irrespective of the complexes' topology, we note the significantly larger band intensities for the para form as opposed to those for the meta isomer. The new absorptions in the optical and the near-infrared (near-IR) spectra resemble the lower energy absorptions of the radical anions (or cations) of 1,2-diphenylethylene and 1,4-distyrylbenzene, which are commonly referred to as the A_1 and A_2 or C_1 and C_2 bands, respectively. These organic radical cations and anions have been thoroughly investigated as models of the polarons that exist in the charged states of conducting polymers based on oligo- and poly(phenylenevinylene) (OPV, PPV).[51,54−58] Vibrational spacings of ca. 1600 cm^{-1} for the higher energy band and of 1420 and 1165 cm^{-1} for the lower energy band have been observed for **m-2**$^+$ and **p-2**$^+$ (see footnotes *b* and *e* of Table 2), and these are again similar to those observed for OPV radical cations and anions.[55,56] It is interesting to note that these bands appear at energies somewhat higher (higher energy band) or very similar to (lower energy band) those for the radical anion derived from diphenylethene (E_{op} = 15 727 and 8307 cm^{-1}). The similarities in both band shape and positions argue for a predominantly ligand-centered oxidation in the case of the P^iPr_3-containing diruthenium complexes **m-2** and **p-2**.

Further conversion from the mono- to the dioxidized forms also led to distinct changes in the electronic spectra. As is depicted in Figure 3, the vibrationally structured bands in the visible and near-IR regions disappear while new, unstructured bands at 396 and 626 nm (**m-2**$^{2+}$) or at 430 and 624 nm (**p-2**$^{2+}$) grow in. There are again clean isosbestic points at 347, 1006, and 1393 cm^{-1} (**m-2**$^+$ → **m-2**$^{2+}$), and at 318, 383, 466, and 860 nm (**p-2**$^+$ → **p-2**$^{2+}$). The band around 625 nm is similar for both isomers in terms of position and intensity; it accounts for the intense blue color of the dications. In contrast, there are profound differences between the two isomers with regard to the band at higher energy. This band becomes the dominant absorption in the visible region for **m-2**$^{2+}$ but is only of low intensity in the case of **p-2**$^{2+}$. Again we note similarities of the optical spectra from the dications **m-2**$^{2+}$ and **p-2**$^{2+}$ with those of the purely organic counterparts. Thus, the dioxidized form of the 2,5-distyrylthiophene dication absorbs at 511 nm, while maxima at 512 and 700 nm in heavily doped poly(phenylenevinylene) serve as a benchmark for highly delocalized divinylphenylene- or distyrylbenzene-derived dications.[55,56]

IR Spectroelectrochemistry. We next sought to probe the extent of the metal contribution to the SOMO by means of IR spectroelectrochemistry. Owing to the prototypical π-acid properties of the carbonyl ligand, the redox-induced CO stretching band shifts faithfully mirror the electron density changes at the metal. As an additional feature, IR spectroscopy of dinuclear carbonyl complexes also provides a convenient means to probe the intrinsic charge and valence delocalization: i.e., identity (symmetry) or nonidentity (asymmetry) of the bridged metal sites. The stronger the electronic coupling between the carbonyl bearing metal entities, the more the CO band positions of each subunit in the mixed-valent state will deviate from the position in a related mononuclear complex (in the respective redox state) and the more closely the CO energies of the individual subunits will resemble each other.

Sequential oxidation of **m-2** in an OTTLE cell first led to the replacement of the single band of the neutral form at 1910 cm^{-1} by two equally intense features at 1915 and 1971 cm^{-1} (Figure 4a). At the same time, the HC═CH stretching bands of the divinylphenylene bridge shift from 1577 and 1554 cm^{-1} to 1523 cm^{-1}, along with a significant gain in intensity. Upon the second oxidation, the two CO bands of **m-2**$^+$ merge into a single band at 1983 cm^{-1}, again with a clean isosbestic point (Figure 4b).

When **p-2** was oxidized to the monocation, the original CO stretching band at 1910 cm^{-1} was gradually replaced by a structured band with an apparent maximum at 1932 cm^{-1} and

(53) Krejcik, M.; Danek, M.; Hartl, F. *J. Electroanal. Chem. Interfacial Electrochem.* **1991**, *317*, 179.
(54) Heidenreich, A.; Münzel, N.; Schweig, A. *Z. Naturforsch.* **1986**, *41a*, 1415.
(55) Deussen, M.; Bässler, H. *Chem. Phys.* **1992**, *164*, 247.
(56) Bässler, H.; Deussen, M.; Heun, S.; Lemmer, U.; Mahrt, R. F. *Z. Phys. Chem.* **1994**, *184*, 233.
(57) Sakamoto, A.; Furukawa, Y.; Tasumi, M. *J. Phys. Chem.* **1994**, *98*, 4635.
(58) Sakamoto, A.; Furukuwa, Y.; Tasumi, M. *J. Phys. Chem.* **1992**, *96*, 3870.

Table 2. Spectroscopic Parameters of m-2 and p-2 in Various Oxidation States

	IR ν, cm^{-1} ($1480-2200\ cm^{-1}$)	UV/vis λ_{max}, nm (ϵ_{max}, $10^{-3}\ M^{-1}\ cm^{-1}$)	ESR A, G ($=10^{-4}$ T)
m-2	1910, 1577, 1554	308 (16.6), 377 (sh, 4.7), 513 (0.87)	
m-2$^+$	1971, 1915, 1524	308 (15.3), 386 (sh, 3.56), 531 (1.84),[a] 1265 (1.80),[b] 2330 (0.51)[c]	$T = 230$ K: $g_{iso} = 2.0274$ $A(^1H) = 10$ (2 H), 8 (2 H); $A(^{99/101}Ru) = 6$ $T = 110$ K: $g = 2.0113$
m-2^{2+}	1983	309 (15.7), 396 (12.3), 626 (6.03)	
p-2	1910, 1573, 1561	353 (10.3), 405 (2.63), 503 (1.33)	
p-2$^+$	1942, 1932, 1915, 1519, 1503, 1481	346 (5.82), 585 (4.27),[d] 1255 (4.11)[e]	$T = 293$ K: $g_{iso} = 2.0278$ $A(^1H) = 9.5$ (2 H), 8 (2 H); $A(^{99/101}Ru) = 4.5$ $T = 110$ K: $g = 2.0221$
p-2^{2+}	1991	266 (9.06), 430 (3.23), 624 (5.36)	

[a] Data for main peak; resolved progressions at 489 and 581 nm. [b] Data for main peak; resolved progressions at 928 and 1078 nm. [c] Data for main peak from deconvolution (see text). [d] Data for main peak; deconvolution gives additional progressions at 492 and 535 nm. [e] Data for main peak; deconvolution gives additional progressions at 949 and 1067 nm.

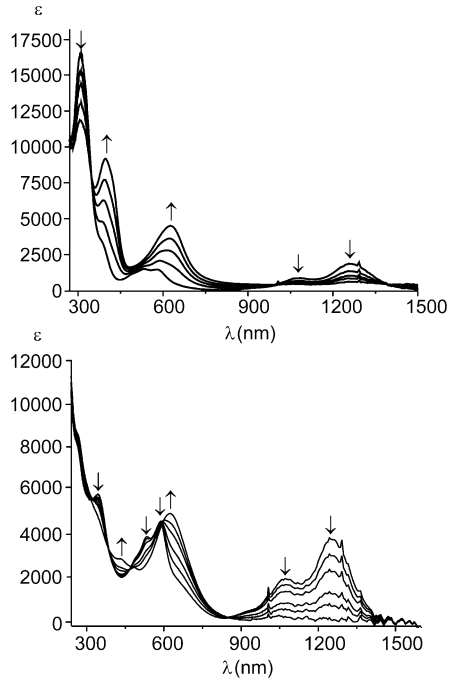

Figure 3. UV/Vis/near-IR spectroelectrochemical traces recorded during the second oxidation of **m-2** (upper graph) and **p-2** (lower graph).

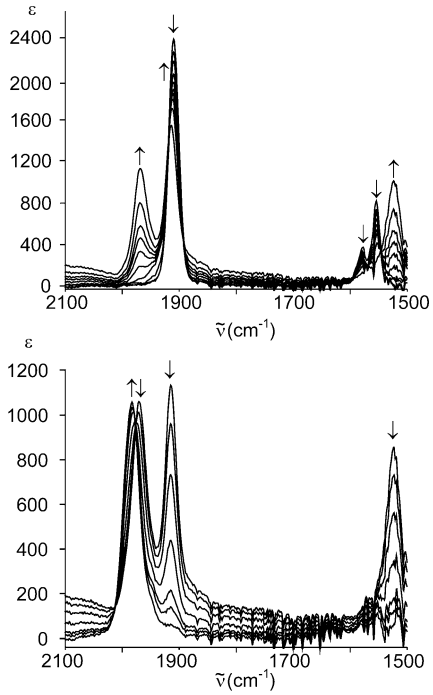

Figure 4. IR spectroelectrochemistry of **m-2** in DCE/NBu_4PF_6 at 295 K: (upper graph) first oxidation; (lower graph) second oxidation.

additional high- and low-energy shoulders (Figure 5a). Spectral deconvolution placed the individual peaks at 1915, 1932, and 1942 cm^{-1}, while indicating that the shoulders are associated with band half-widths and areas larger than for the 1932 cm^{-1} feature. Solutions prepared by quantitative coulometry in a conventional bulk electrolysis cell displayed an identical band pattern (Figue S2, vide infra). The overall band shape thus points to the presence of two coexisting species in solution. As a possible explanation, we invoke two distinct rotamers that differ with respect to the orientation of the {Ru(CO)Cl} subunits: i.e., a cisoid or transoid arrangement of the carbonyl groups (see Chart 2). DFT calculations indicate that both these rotamers correspond to minima on the potential energy surface with only a small energy difference between them.[59] The three-band pattern may then arise form an overlap between two pairs of bands for the different rotamers or from that of a two-band pattern for the major isomer and a single-band pattern for the minor isomer.[60] As the oxidation proceeds, the weak HC═CH bands of **p-2** at 1573 and 1561 cm^{-1} give way to much stronger absorptions at 1519, 1503, and 1481 cm^{-1} of **p-2**$^+$. During the second anodic step the band(s) of the monocation are replaced by just one CO band for the fully oxidized dication **p-2**$^{2+}$, which is now located at 1991 cm^{-1} (Figure 5b). The energy of the HC═CH/PhC═C bands decreased further such that they were shifted to a range where the NBu_4^+ cation of the supporting electrolyte absorbs strongly. It was thus impossible to determine the peak position of these bands for **p-2**$^{2+}$ from IR spectroelectrochemistry.

(59) The calculated energies represent gas-phase values. Relative energies of both rotamers will be different in solution, owing to the differences in the dipole moments (none for the transoid and ca. 3.19 D for the cisoid conformation of **m-2**). A polar environment is thus expected to even decrease the energy difference between these rotamers.

(60) One should note that any dinuclear complex featuring two monocarbonylmetal entities should give rise to two nondegenerate CO bands representing the symmetrical and antisymmetrical combinations of the individual M−CO stretches. Calculated IR spectra for the two rotamers of **m-2** and **p-2** in any of its oxidation states consequently give two closely spaced bands with separations in the range of some 4−10 cm^{-1} for each pair of bands. Only one band is, however, experimentally observed for both neutral and dioxidized forms. Obviously broadening due to solute/solvent interactions and rotational averaging reduces the band splitting beyond recognition. The calculated larger CO band energy difference for **m-2**$^{2+}$ nevertheless agrees nicely with the notably large CO bandwidth of this dication observed in our experiments.

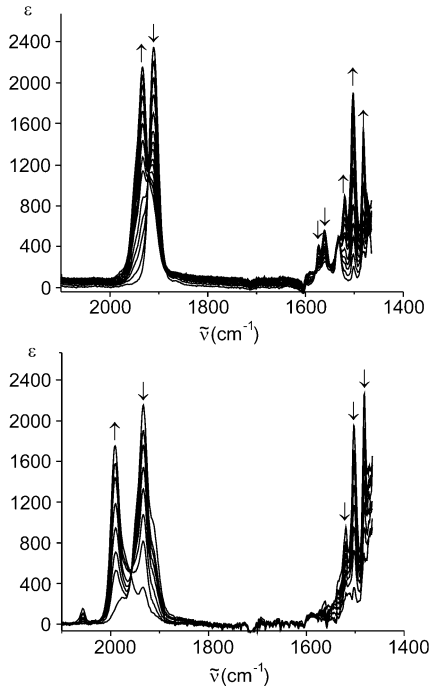

Figure 5. IR spectroelectrochemistry of **p-2** in DCE/NBu_4PF_6 at 295 K: (upper graph) first oxidation; (lower graph) second oxidation.

Chart 2

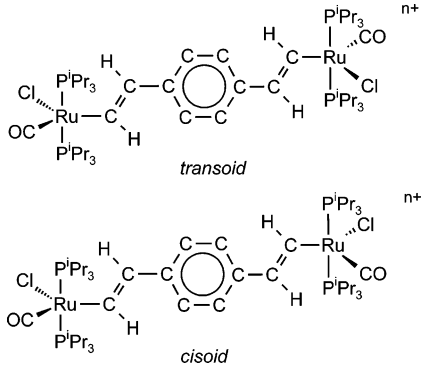

Three points are of special interest.

(i) The overall CO band shift upon twofold oxidation of complexes **m-2** (73 cm^{-1}) and **p-2** (71 cm^{-1}) is consistently larger than that of the $\{(PPh_3)_2(CO)Cl(pyR)Ru\}_2(\mu\text{-}HC{=}CHC_6H_4CH{=}CH)$ counterparts (ca. 45 cm^{-1}). This attests to higher contribution from the ruthenium entities to the redox orbitals of **m-2**$^{n+}$ and **p-2**$^{n+}$, owing to the higher d-orbital energies in the more electron rich P^iPr_3-containing complexes. The larger CO band shift upon oxidation may, however, also rely on the absence of the pyridine ligand, which, as the only weak π-acceptor, can serve to buffer the loss of electron density at the metal in the six-coordinated congeners. There are indeed small, yet clearly notable shifts of the ester bands of the isonicotinate ligands (R = COOEt) for the PPh_3-derived complexes.

(ii) The average shifts of the CO stretching bands for the first oxidation step are consistently smaller than those for the second oxidation process. With an average value of 33 cm^{-1} for the first and of 40 cm^{-1} for the second oxidation step, the difference is only moderate for **m-2**. For **p-2**, however, the average shift difference is much more pronounced at ca. 20 cm^{-1} as opposed to 60 cm^{-1}. This may indicate that the metal contribution to the respective frontier orbital increases with the overall oxidation state, especially for the para isomer. In fact, DFT calculations indicate that the metal contribution to the redox orbital increases from 25% to 31% when going from **p-2** to **p-2**$^{2+}$.

(iii) Two widely spaced CO stretching bands are present for the monocation **m-2**$^+$ ($\Delta\nu = 56$ cm^{-1}), the one at lower energy being only slightly shifted from the position in **m-2** and the one at higher energy being moderately shifted from that of **m-2**$^{2+}$, and two more closely spaced absorptions for the major form of **p-2**$^+$ ($\Delta\nu = 27$ cm^{-1}), indicating that these isomers differ significantly with respect to the charge distribution across the metal sites. We note here that the relative shifts of the CO bands in the mixed-valent form in comparison to the neighboring homovalent states provide the charge distribution parameter $\Delta\rho$, which constitutes a quantitative measure for the extent of valence delocalization.[61,62] The latter is defined as

$$\Delta\rho = (\Delta\nu_{ox} - \Delta\nu_{red})/2[\nu'(ox) - \nu'(red)] \qquad (1)$$

where ν'(ox) and ν'(red) denote the CO stretching wavenumbers of the fully oxidized and the fully reduced forms while $\Delta\nu_{ox}$ and $\Delta\nu_{red}$ are the energy differences between the band positions of the fully oxidized species and the higher energy band of the monooxidized form and between the lower energy band of the intermediate and that of the fully reduced form, respectively.[61,62] The $\Delta\rho$ parameter is expected to increase with increasing metal−metal interactions in the mixed-valent state, approaching values of 0.5 in the completely delocalized case (class III) and a value of 0.0 in the completely localized limit (class I). This model works under the premise that the metal contribution to the corresponding frontier orbitals remains constant throughout the oxidation processes under consideration, which may not necessarily be the case here. A $\Delta\rho$ value of 0.12 was calculated for **m-2**$^+$, whereas that of 0.31 for **p-2**$^+$ is significantly larger. The latter value was derived under the assumption that the outermost features of the composite CO band belong to the same species. In other words, the charge is more evenly spread across the entire dimetal−divinylphenylene unit in **p-2**$^+$ but is distinctly localized on half of the molecule in **m-2**$^+$. This finding is consistent with what is known from phenylenevinylene-derived polarons. While in the para-linked oligomers charge and spin are delocalized over rather long distances,[56,63,64] the meta isomers tend to have localized charge and spin on just one styryl unit.[64]

ESR Spectroscopy. ESR spectroscopy constitutes a highly sensitive method in order to elucidate the metal versus (organic) ligand contributions to the SOMO of paramagnetic species. Such information can be obtained from the isotropic *g* values, from the **g**-tensor anisotropy measured in glassy frozen solutions or solid samples, and from the hyperfine coupling, either to the metal atom(s) or to other ESR-active nuclei of coordinated ligands. With ruthenium as the metal, the situation is far from ideal: rapid relaxation often renders Ru(III) species ESR silent in fluid solution, and hyperfine splitting to ^{101}Ru or ^{99}Ru (17.0 and 12.7%, respectively; $I = {}^5/_2$) may be too small to be observed in the frozen state. The intense ESR signals of **m-2**$^+$ and **p-2**$^+$ around $g_{iso} \approx 2.028$ in fluid solution make therefore a strong case for ligand-dominated oxidation underpinning the results from UV/vis and IR spectroelectrochemistry. Interest-

(61) Stoll, M. E.; Lovelace, S. R.; Geiger, W. E.; Schimanke, H.; Hyla-Kryspin, I.; Gleiter, R. *J. Am. Chem. Soc.* **1999**, *121*, 9343.
(62) Atwood, C. G.; Geiger, W. E. *J. Am. Chem. Soc.* **2000**, *122*, 5477.
(63) Rauscher, U.; Bässler, H.; Bradley, D. D. C.; Hennecke, M. *Phys. Rev. B* **1990**, *42*, 9830.
(64) Karabunarliev, S.; Baumgarten, M.; Tyutyulkov, N.; Müllen, K. *J. Phys. Chem.* **1994**, *98*, 11892.

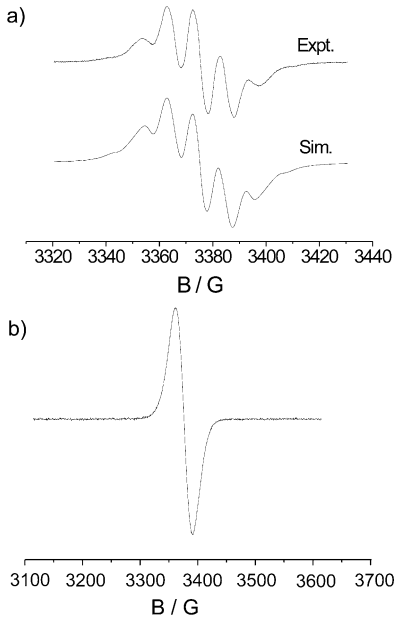

Figure 6. ESR spectra of electrogenerated **p-2**$^+$ in CH_2Cl_2/NBu_4PF_6: (a) in fluid solution at 293 K, experimental spectrum (upper trace) and simulated spectrum (lower trace, see text); (b) experimental spectrum at 110 K.

ingly, both **m-2**$^+$ and **p-2**$^+$ exhibit resolved hyperfine splitting to the vinyl protons and to the ruthenium nuclei. Experimental spectra were well reproduced by simulations when three different coupling parameters were applied: one for the vinylic protons at the metal-bonded carbon atom, one for the protons at the vinylic carbon atom which connects to the central phenylene unit, and one for two equivalent ruthenium nuclei. Figure 6a compares the experimental and simulated spectra of **p-2**$^+$. Spectra recorded in glassy frozen solution display only a single broad resonance line without discernible *g* anisotropy at X-band frequency (9.5 GHz). A certain contribution from the ruthenium atoms to the SOMO is nevertheless indicated by the relatively high isotropic *g* values in fluid solution and in frozen samples (see Table 2). Organic ligand-centered radicals are characterized by *g* values close to that of the free electron at 2.0023. The deviations observed for **m-2**$^+$ and **p-2**$^+$ from this value are therefore indicative of nonnegligible metal contribution to the SOMO. We also note that g_{iso} values of **m-2**$^+$ and **p-2**$^+$ are slightly larger than the value of 2.020 measured for (*E*,*E*)-[{$(PPh_3)(CO)(Cl)$(4-EtOOCpy)Ru}$_2$(μ-CH═CH−C_6H_4CH═CH-1,3)], again in line with some larger metal contribution for the P^iPr_3-substituted congeners. Our results thus point to an essentially ligand-centered oxidation and a +II oxidation state for the ruthenium atoms for **m-2**$^+$ and **p-2**$^+$. Apart from being ESR silent in fluid solution, organometallic paramagnetic Ru(III) species usually display much larger *g* value anisotropies in their frozen-solution spectra and substantially larger deviations of the isotropic *g* value from that of the free electron. Typical examples are the alkynyl complexes [$(Me_2bipy)(PPh_3)_2ClRu(C{\equiv}CR)$]$^+$ [65] and allenylidene complexes [$Cl(dppm)_2Ru${═C═C═C(NRR′)-(but-3-enyl)]$^{2+}$,[34] where the g_{iso} values range from 2.127 to 2.170 with *g* value anisotropies larger than 0.5.

One finding deserves further mention here. While the radical cation **m-2**$^+$ of the meta isomer is clearly unsymmetrical on the vibrational time scale of 1×10^{-11} to 1×10^{-12} s, it appears to be symmetrical on the slower ESR time scale of 1×10^{-9} to 1×10^{-8} s. In fact, solution ESR spectra of **m-2**$^+$ (see Figure S1 of the Supporting Information) and **p-2**$^+$ are nearly superimposable, with only slightly different hyperfine coupling constants. This parallels the phenomenon of time-dependent valence detrapping, where the assignment of a mixed-valent system as either fully delocalized class III or localized class II depends on the time scale of the experiment.[62,66,67] In mixed-valent chemistry, such behavior is typical of systems that are close to the interesting borderline between these two regimes.[68,69] In the case of **m-2**$^+$, however, it may indicate a time-dependent localization of charge and spin on predominantly one styryl subunit or delocalization over both styryl subunits.

Quantitative Coulometry. Spectroelectrochemistry allows us to simultaneously generate and spectroscopically investigate oxidized or reduced forms associated with a redox-active compound. It is an important merit of this in situ approach that it may extend the detection limits to quite reactive oxidized or reduced species that might otherwise escape detection under the conditions of conventional bulk electrolysis.[70,71] There is, however, the possibility that chemically reversible behavior in spectroelectrochemical experiments conceals some intricate chemistry following electron transfer. As long as the overall chemical reversibility is maintained upon completing a full oxidation/reduction cycle and redox-induced interconversions are fast, chemical processes such as redox-induced isomerizations[72] may well go unnoticed under the conditions of spectroelectrochemistry.

To confirm the results obtained for **m-2** and **p-2**, we supplemented the spectroelectrochemical studies conducted within the OTTLE cell (UV/vis/near-IR, IR) or via in situ ESR spectroscopy by bulk electrolyses inside a conventional electrolysis cell. In each case, the working potential was adjusted to about 150 mV positive to the half-wave potential of the first anodic wave, and electrolysis was continued until the current had dropped to about 2% of the initial value. At this stage close to 1 faraday/mol of charge had been transferred, in accordance with the proposed one-electron nature of each redox wave. During electrolysis the color of the originally orange-red solutions intensified to deep green (**m-2**$^+$) or intense purple (**p-2**$^+$). Voltammograms recorded after the first oxidation step are complementary to those of the nonoxidized forms, except for the observation that the wave at lower potential now appeared as a reduction wave. Close comparison revealed the presence of an additional couple at a potential higher than that of any of the original analyte waves. The associated peak currents are, however, small and increase just slightly upon repetition of a full reduction/reoxidation cycle. This indicates that the singly oxidized forms are rather stable in solution at ambient temperature, even on the extended time scale (ca. 30 min) of bulk electrolyses. Samples were removed from the working electrode compartment after monooxidation was completed and their IR, UV/vis/near-IR, and ESR spectra recorded. The obtained spectra

(65) Adams, C. J.; Pope, S. J. A. *Inorg. Chem.* **2004**, *43*, 3492.

(66) Atwood, C. G.; Geiger, W. E.; Rheingold, A. L. *J. Am. Chem. Soc.* **1993**, *115*, 5310.

(67) Ito, T.; Hamaguchi, T.; Nagino, H.; Yamaguchi, T.; Kido, H.; Zavarine, I. S.; Richmond, T.; Washington, J.; Kubiak, C. P. *J. Am. Chem. Soc.* **1999**, *121*, 4625.

(68) Lambert, C.; Nöll, G. *J. Am. Chem. Soc.* **1999**, *121*, 8434.

(69) Nelsen, S. F. *Chem. Eur. J.* **2000**, *6*, 581.

(70) McCreery, R. L. Spectroelectrochemistry. In *Electrochemical Methods*; Rossiter, B. W., Hamilton, J. F., Eds.; Wiley: New York, 1986; Vol. II, p 591.

(71) Alessio, E.; Daff, S.; Elliot, M.; Iengo, E.; Jack, L. A.; Macnamara, K. G.; Pratt, J. M.; Yellowlees, L. J. Spectroelectrochemical techniques. In *Trends in Molecular Electrochemistry*; Pombeiro, A. J. L., Amatore, C., Eds.; Marcel Dekker: Lausanne, New York, 2004; p 339.

(72) Pombeiro, A. J. L.; Guedes da Silva, M. F. M. C.; Lemos, M. A. N. D. A., *Coord. Chem. Rev.* **2001**, 219−221, 53.

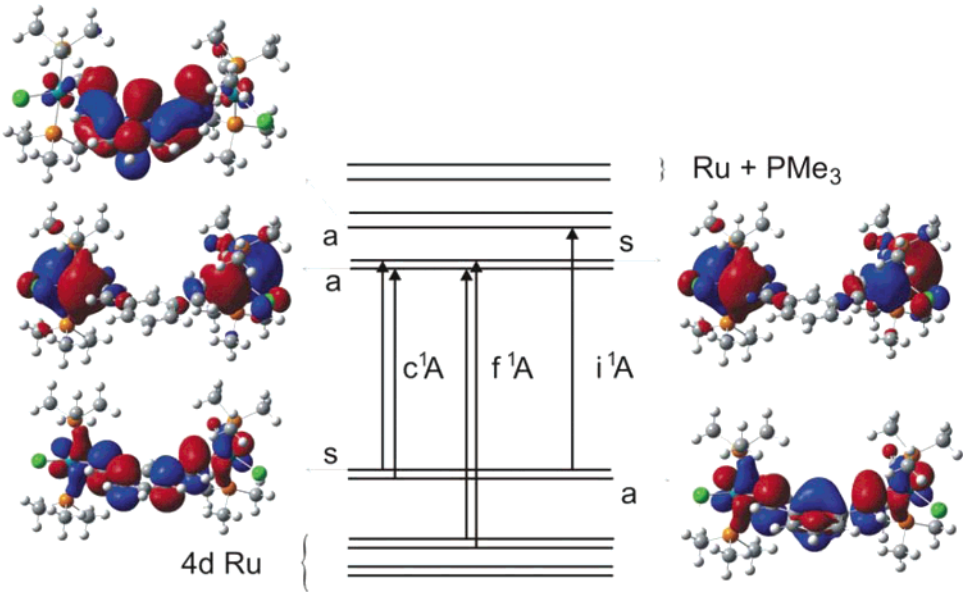

Figure 7. Qualitative MO scheme of **m-2^{Me}**. Arrows indicate the main contributions to the lowest allowed TD DFT calculated transitions. The letters **s** and **a** label the symmetric and antisymmetric combinations of 4d Ru orbitals, respectively.

were essentially identical with those observed under the conditions of spectroelectrochemistry (see Figures S2 and S3 in the Supporting Information). When we then performed the second oxidation, the color of the solution rapidly changed to deep blue and optical spectra recorded at this point showed the 625 nm absorption peak of the dioxidized forms. When electrolyses were continued, the color gradually faded and decomposition was indicated by the disappearance of the initial redox waves. The fully oxidized solutions displayed a single anodic wave which is identical with that observed as a minor constituent after the first oxidation step. Samples taken from the decomposed oxidized solution did not show any significant absorption in the carbonyl stretching region of the IR spectrum. This is highly suggestive of a decarbonylation or demetalation process underlying the decomposition. While our bulk electrolysis studies thus confirm the one-electron nature of each voltammetric wave and the results obtained in the spectroelectrochemical investigations, they also demonstrate the superior performance of the in situ approach when reactive redox congeners are involved.

Quantum-Chemical Calculations. Quantum-chemical calculations based on density functional (DFT) methods (see Experimental Section) were performed in order to address the issues of (i) comparing the electronic structures of the meta and para isomers, (ii) assessing the geometrical structures and the degree of torsion around the metal−vinyl and central phenylene units, (iii) probing the effect of coordinative unsaturation of the metal as opposed to the case for the six-coordinate pyridine adducts, especially with respect to the LUMO and LUMO+1 levels, (iv) comparing the calculated and experimental spectroscopic parameters for these derivatives at their various oxidation levels, and (v) probing the oxidation-state-dependent metal contribution to the frontier orbitals, as was suggested by the varying CO band shifts in IR spectroelectrochemistry. For the sake of reducing the computational effort, the actual systems were simplified by replacing the P^{i}Pr$_3$ ligands by PMe$_3$. These model systems are denoted as **m-2^{Me}** and **p-2^{Me}**, respectively.

Figures 7 and 8 provide the MO schemes of **m-2^{Me}** and **p-2^{Me}** in the frontier orbital region along with contour plots of the most important orbitals, while the contributions of the individual constituents to the respective orbitals as based on a Mulliken analysis are given in Tables S1 and S2 in the Supporting Information. As is evident from these figures and tables, the isomers closely resemble each other with respect to the composition of the frontier orbitals that are relevant for their optical and electrochemical properties. The HOMO and HOMO-1 levels have large contributions from the π_3 levels of the divinylphenylene ligand interacting with the appropriate combination of d orbitals at the metal atoms. In the case of **m-2^{Me}**, the HOMO and HOMO-1 orbitals are nearly degenerate, with an energy gap of just 0.22 eV. In contrast, the separation of these levels is 0.97 eV for **p-2^{Me}**. Below is an again nearly isoenergetic set derived from the symmetrical and antisymmetrical combinations of {Ru(CO)Cl}-based orbitals with only very little contribution from the bridge. Despite the vacancy of the sixth coordination site, the unoccupied frontier orbitals, LUMO and LUMO+1, are still very much centered on the metal end groups and are of a mainly Ru/phosphine parentage. The LUMO+2 essentially is a π-level of the divinylphenylene bridge with only minor contributions from the ruthenium moieties.

Geometry optimizations of the **m-2^{Me}** and **p-2^{Me}** model complexes in their various oxidation states reveal the impact of the redox processes on the structures. Table 3 gives the important bond parameters calculated for neutral systems. Related five-coordinated mononuclear styryl or vinyl complexes[73−78] may serve as points of comparison for the neutral forms. The overall agreement between the calculated and experimental values for the vinyl complexes containing {M(CO)Cl(PR$_3$)$_2$} is quite good. The corresponding parameters of the meta divinylphenylene ligand are best compared with those of the trivinylphenylene-bridged diruthenium complex [{(Ph$_3$P)$_2$(py)(CO)ClRu}$_3$(μ-HC═CH)$_3$C$_6$H$_3$-1,3,5] reported by

(73) Alcock, N. W.; Cartwright, J.; Hill, A. F.; Marcellin, M.; Rawles, H. M. *J. Chem. Soc., Chem. Commun.* **1995**, 369.
(74) Torres, M. R.; Vegas, A.; Santos, A. *J. Organomet. Chem.* **1986**, *309*, 169.
(75) Werner, H.; Esteruelas, M. A.; Otto, H. *Organometallics* **1986**, *5*, 2295.
(76) Wakatsuki, Y.; Yamazaki, H.; Kumegawa, N.; Satoh, T.; Satoh, J. Y. *Organometallics* **1991**, *113*, 9604.
(77) Maruyama, Y.; Yamamura, K.; Sagawa, T.; Katayama, H.; Ozawa, F. *Organometallics* **2000**, *19*, 1308.
(78) Jung, S.; Ilg, K.; Brandt, C. D.; Wolf, J.; Werner, H. *Eur. J. Inorg. Chem.* **2004**, 469.

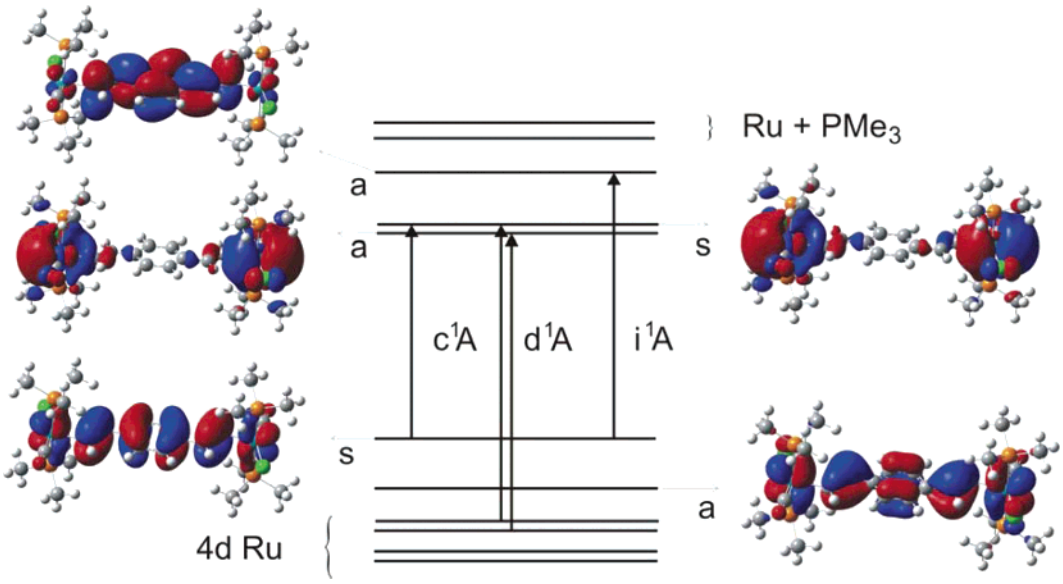

Figure 8. Qualitative MO scheme of **p-2^{Me}**. Arrows indicate the main contributions to the lowest allowed TD DFT calculated transitions. The letters **s** and **a** label the symmetric and antisymmetric combinations of 4d Ru orbitals, respectively.

Table 3. G03/B3LYP Calculated Symmetry-Averaged Bond Lengths (Å) and Angles (deg) for the Model Compounds m-2^{Me} and p-2^{Me} in Comparison with Experimental Data[a]

	m-2^{Me}		**p-2^{Me}**
	calcd	exptl[a]	calcd
Ru−C(CO)	1.822	1.810	1.823
Ru−Cl	2.457	2.467	2.458
Ru−C_1	2.037	2.044	2.036
Ru−P	2.388	2.396	2.389
C_1−C_2	1.349	1.323	1.351
C_2−C_3	1.479	1.472	1.474
C_3−C_4	1.404	1.389	1.412
C_4−C_5	1.393	1.393	1.443
C−O	1.170	1.139	1.170
Ru−C_1−C_2	122.6	135.1	121.8
C_1−C_2−C_3	126.9	127.3	127.5
C_1−C_2−C_3−C_4	13.0	14.4	0.1

[a] Average values from ref 79 for [{$(Ph_3P)_2$(py)(CO)ClRu}$_3$(μ-HC═CH)$_3$-C_6H_3-1,3,5].

Jia and co-workers.[79] The latter, however, contains six-coordinate metal centers. We also note the close agreement with respect to the dihedral angles between the central benzene ring and the vinyl groups of **m-2** (calculated value, 13°; experimental values, 13.3−15.0°).[79] The calculated dihedral angle for **p-2^{Me}** approaches 0°. Upon sequential oxidation we note a stepwise shortening of the Ru−C (average Δr(Ru−C) ≈ 0.07 Å) and C_{Ph}−C_{vinyl} bonds ($\Delta r \approx 0.03$ Å) and a concomitant lengthening of the former vinylic C═C bonds ($\Delta r \approx 0.03$ Å) for each oxidation step (see Tables S3 and S4 in the Supporting Information). This agrees well with the observed red shift of $\nu_{C=C}$ in IR spectroelectrochemistry. There is also some quinoidal distortion of the central phenylene ring that increases with the overall oxidation state. Similar observations have been made for the mono- and dioxidized forms of tetraphenylethenes[80,81] and for the various reduced forms of *m*- and *p*-phenylene-vinylenes.[64] Note that in these latter systems oxidation and reduction have very similar effects on the structural and spectroscopic properties.[55,57,58,63,82] Other structural changes of the Ru(CO)Cl$(PMe_3)_2$ moiety upon oxidation consist of a slight lengthening of the Ru−P bonds and a shortening of the Ru−Cl bonds, indicating the loss of some electron density from the metal. Alterations of these parameters are, however, considerably smaller than one would expect for the loss of a full unit charge from the metal.[83−85] All of these data, along with the overall composition of the HOMO and HOMO-1 orbitals, point to a strong involvement of the divinylphenylene bridge in the oxidation processes. Electron density difference plots for the 0/+ states (+/2+ density difference plots are similar), as are depicted in Figure S4 in the Supporting Information, nicely confirm these findings and are strongly supportive of our experimental results. They show that the loss of electron density from the organic π-system (40.7% for the first and 28.0% for the second oxidation of **m-2**, 38.2% for the first and 27.6% for the second oxidation of **p-2**) largely outweighs that of the ruthenium centers (13.3 and 9.5% for **m-2**, 11.3 and 10.6% for **p-2**) for both oxidation steps, regardless of the topology of the bridge. We also note that the DFT calculations predict that the doubly oxidized para isomer possesses a singlet ground state with the triplet state lying ca. 0.5 eV higher in energy. In contrast to this, the meta isomer has a triplet ground state with an energy difference to the higher lying singlet state of 0.15 eV.

Spectroscopic parameters were calculated for the **p-2^{Me}** and **m-2^{Me}** models of the P^{i}Pr$_3$ complexes in their various oxidation states. Table 4 lists the calculated stretching frequencies for both compounds in their most stable transoid forms, i.e. the form with the chloro and carbonyl ligands at opposite sides, for all oxidation states. Preliminary calculations indicate that differences in the cisoid forms are negligibly small. As for the ν_{CO}

(79) Xia, H.; Wen, T. B.; Hu, Q. Y.; Wang, X.; Chen, X.; Shek, L. Y.; Williams, I. D.; Wong, K. S.; Wong, G. K. L.; Jia, G. *Organometallics* **2005**, *24*, 562.

(80) Rathore, R.; Lindeman, S. V.; Kumar, A. S.; Kochi, J. K. *J. Am. Chem. Soc.* **1998**, *120*, 6931.

(81) Sun, D.-L.; Rosokha, S. V.; Lindeman, S. V.; Kochi, J. K. *J. Am. Chem. Soc.* **2003**, *125*, 15950.

(82) Obierski, J. M.; Greiner, A.; Bässler, H. *Chem. Phys. Lett.* **1991**, *184*, 391.

(83) Al Salih, T.; Duarte, M. T.; Frausto da Silva, J. J. R.; Galvão, A. M.; Guedes da Silva, M. F. C.; Hitchcock, P. B.; Hughes, D. L.; Pickett, C. J.; Pombeiro, A. J. L.; Richards, R. L. *J. Chem. Soc., Dalton Trans.* **1993**, 3015.

(84) Guedes da Silva, M. F. C.; Ferreira, X. M. P.; Fraústo da Silva, J. J. R.; Pombeiro, A. J. L. *J. Chem. Soc., Dalton Trans.* **1998**, 439.

(85) Carvalho, M. F. N. N.; Duarte, M. T.; Galvão, A. M.; Pombeiro, A. J. L.; Henderson, R.; Fuess, H.; Svoboda, I. *J. Organomet. Chem.* **1999**, *583*, 56.

Table 4. Selected G03/BPW91 Calculated Stretching Frequencies (cm^{-1}) for m-$2^{Me\ n+}$ and p-$2^{Me\ n+}$

	frequency	$n = 0$	$n = 1$	$n = 2$
m-$2^{Me\ n+}$	ν_1 (CO)	1924.7	1948.5	1978.2
	ν_2 (CO)	1928.2	1958.9	1987.2
	ν_1 (CC)	1546.5	1491.5	1477.9
p-$2^{Me\ n+}$	ν_1 (CO)	1925.9	1955.8	1986.8
	ν_2 (CO)	1927.3	1960.5	1990.8
	ν_1 (CC)	1555.2	1513.5	1519.9

values, the calculations reproduce the overall behavior of the CO bands rather well in that they predict a stepwise shift to higher energies as the oxidation state increases. One should note here that two CO bands are calculated for each isomer in every oxidation state. They correspond to the symmetrical (ν_1) and the antisymmetrical (ν_2) combinations of the CO stretching vibrations, which are obviously nondegenerate. The ν_1 and ν_2 frequencies are rather close and are probably not resolved in solution. The presence of various conformers in solution owing to rotation of the $\{Ru(P^iPr_3)_2(CO)Cl\}$ entities around the Ru−vinyl bonds may also contribute to some broadening of the CO bands. Our observation of just one band in the neutral forms and the dications is therefore still compatible with the computational results. A major discrepancy between calculated and experimental data, however, arises in the case of **m-2^+**. Quantum chemistry gives ν_1 and ν_2, which differ by just about 10 cm^{-1}, practically the same value as for the dication. This implies a symmetrical structure of the radical with electronically equivalent $\{Ru(CO)Cl(PR_3)_2(vinyl)\}$ moieties, in stark contrast to the experimental results. The much larger separation observed by IR spectroelectrochemistry indicates two rather distinct metal moieties, one of them resembling the reduced state and the other the fully oxidized state. This inherent unsymmetry of the radical cation **m-2^+** is thus not adequately reproduced by the present calculations. Considering the well-known preference of the DFT method for symmetrical structures and electron distributions, this result is not wholly unexpected. It also suggests that the calculated structural parameters of **m-2^+** are more or less the average of distinct and dissimilar halves of the molecule. We are going to address this issue by applying the broken symmetry approach. In agreement with experiment, the calculations also predict a stronger overall effect on the CO band shift for the second oxidation and nicely reproduce the shift of the HC═CH band upon sequential oxidation. Atom displacements that accompany this vibration have been calculated and are shown in Figure S5 in the Supporting Information. They clearly prove a combined HC═CH stretch and ═CH bend origin of this fundamental.

ESR parameters calculated for the monooxidized forms of **m-2^+** and **p-2^+** also agree reasonably with the experimental values (Table 2), especially with regard to a small g anisotropy. ADF/BP calculations, including spin−orbit coupling, give the isotropic g value $g_{iso} = 2.039$ and a splitting of the **g** tensor with $g_1 = 2.069$, $g_2 = 2.034$, and $g_3 = 2.016$ for **m-2^{Me+}** and $g_{iso} = 2.029$ and $g_1 = 2.050$, $g_2 = 2.026$, and $g_3 = 2.014$ for **p-2^{Me}**. We note again the significant deviation of the g values from that of the free electron. This finding provides direct evidence for some metal contribution to the SOMO, as is also borne out by the observed carbonyl shifts and the calculated compositions of the SOMO orbitals.

While time-dependent DFT (TD DFT) calculations on the open-shell systems **m-2^+** and **p-2^+** are currently being pursued, we restrict ourselves to the assignment of the optical transitions observed for the neutral forms. Arrows in Figures 7 and 8 indicate the main contributions to the lowest allowed TD DFT

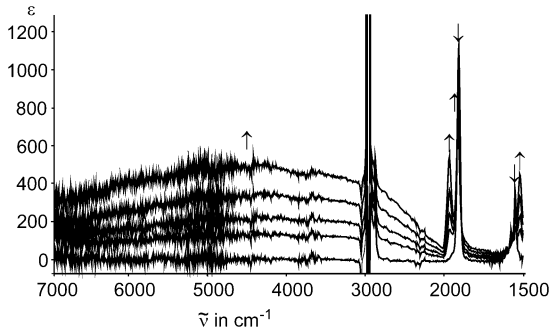

Figure 9. IR spectra recorded during the stepwise oxidation of **m-2** to **m-2^+** on an extended energy scale.

calculated transitions for neutral **p-2^{Me}** and **m-2^{Me}** systems. TD DFT calculations on the model complexes predict weak transitions in the visible region at slightly lower energies than observed (Tables S5 and S6 in the Supporting Information). According to the calculations, this transition involves the set of the closely spaced HOMO/HOMO-1 and LUMO/LUMO+1 levels (c^1A in Figures 7, 8). Considering the composition of these orbitals, the transition may be described as a mixed bridging ligand-to-metal (LMCT) and bridging ligand-to-phosphine (LLCT) electron transfer band. A transition at higher energies which is only visible as a shoulder in the experimental spectra has d−d character (d^1A in Figures 7, 8), while the most intense absorption in the near-UV region can be interpreted as a $\pi \rightarrow \pi^*$ transition within the extended delocalized chromophore (i^1A in Figures 7, 8). TD DFT calculations on closed shell dication **p-2^{2+}** indicate a red shift of the low-energy transition, in agreement with experiment.

Observation of a Low-Energy Electronic Band for m-2^+. When monitoring the spectroscopic changes of vibrational spectra over an extended energy range, we observed the reversible growth (**m-2** → **m-2^+**; see Figure 9) and disappearance (**m-2^+** → **m-2^{2+}**; see Figure S6 in the Supporting Information) of a broad absorption covering the entire range from 7500 to 2000 cm^{-1}. The overall band shape was best reproduced by invoking three overlapping bands at ca. 6550, 4300, and 2950 cm^{-1} with half-widths of 2600, 2100, and 1100 cm^{-1}, respectively. Considerable noise in the experimental spectrum, however, limits the accuracy of the absolute values.

Electronic absorption bands in this energy range are a typical feature of weakly coupled mixed-valent systems where two or more identical or similar redox sites are present in formally different oxidation states. Similar bands have on occasion also been observed for unsymmetrical complexes that combine redox-active metals and "noninnocent ligands" with similar redox potentials as the metal ions. Such bands have either ligand-to-metal (LMCT) or metal-to-ligand (MLCT) character, depending on which of the two possible states, oxidized metal/reduced ligand or reduced metal/oxidized ligand, is energetically more favorable.[86−88] These bands are conceptually important, in that they provide the electronic coupling parameter H_{MM} or H_{LM}, respectively, on the basis of the Hush model.[89−92]

(86) Desjardins, P.; Yap, G. P. A.; Crutchley, R. J. *Inorg. Chem.* **1999**, *38*, 5901.
(87) Mosher, P. J.; Yap, G. A. P.; Crutchley, R. J. *Inorg. Chem.* **2001**, *40*, 1189.
(88) Lloveras, V.; Caballero, A.; Tárraga, A.; Velasco, M. D.; Espinosa, A.; Wurst, K.; Evans, D. J.; Vidal-Gancedo, J.; Rovira, C.; Molina, P.; Veciana, J. *Eur. J.Inorg. Chem.* **2005**, 2436.
(89) Hush, N. S. *Prog. Inorg. Chem.* **1967**, *8*, 391.
(90) Hush, N. S. *Coord. Chem. Rev.* **1985**, *64*, 135.
(91) Creutz, C. *Prog. Inorg. Chem.* **1983**, *30*, 1.

Interpretation of low-energy electronic absorption bands within the framework of this model assumes that electronic excitation involves the transfer of charge, either from the formally reduced to the formally oxidized metal ion or between the metal and the redox-active ligand. The radical cation **m-2**$^+$ probably conforms to none of these cases. Here, the electronic transition in the near-infrared region likely originates from the excitation of an electron from the SOMO-1 level to the SOMO. Preliminary calculations of **m-2**$^+$ suggest that such a transition may be observed. Since the SOMO and SOMO-1 levels of **m-2**$^+$ are both metal−ligand antibonding combinations of the π_3 level of the divinylphenylene ligand and appropriate d orbitals, the low-energy band of **m-2**$^+$ is attributed to a $\pi \rightarrow \pi^*$ type transition. Its appearance in the near-IR/IR regime is then the result of the near-degeneracy of these levels. This parallels the appearance of similar HOMO-$n \rightarrow$ SOMO transitions in the same spectral region for the radical cations of diethynylarylene (arylene = 2,5-thiophenylene, 9,10-anthracenylene)- and octatetraynediyl-bridged diruthenium complexes.[17] A similar band should also be observed for the monoxidized form of the para isomer. In **p-2**$^+$ the energy gap between the SOMO-1 and the SOMO levels is, however, much larger than in **m-2**$^+$ and the corresponding SOMO-1 $\rightarrow$ SOMO transition may thus be obscured by the strong electronic band at 1255 nm. In this context we note that this band is about four times more intense for **p-2**$^+$, as is the case for its meta isomer. The appearance of three overlapping features instead of just one and their large half-widths may point to different rotamers and to large structural reorganization following excitation.

Conclusions

Our investigations on divinylphenylene-bridged diruthenium complexes establish that σ-bonded divinylphenylenes constitute a unique class of noninnocent ligands for organometallic compounds. As is shown by IR, UV/vis/near-IR, and ESR spectroscopy, oxidation of these systems is largely centered on the organic bridge. Comparison of (*E*,*E*)-[{(P^iPr_3)$_2$(CO)ClRu}$_2$-(μ-HC═CHC$_6$H$_4$CH═CH-1,3)] (**m-2**) and (*E*,*E*)-[{(P^iPr_3)$_2$(CO)-ClRu}$_2$(μ-HC═CHC$_6$H$_4$CH═CH-1,4)] (**p-2**) and their PPh_3-substituted counterparts shows how the electronic balance of bridge and metal contribution to the occupied frontier levels can be controlled by the appropriate choice of coligands. Decreasing the gap between the metal d orbitals and the higher lying π levels of the bridge leads to a greater metal character of the oxidized forms. This follows from the larger CO band shifts upon stepwise oxidation of the P^iPr_3-substituted complexes and from the observation of resolved hyperfine splittings between the unpaired spin and the ruthenium nuclei. Replacement of PPh_3 by the more basic P^iPr_3 also stabilizes the partially and fully oxidized forms to such an extent that it was possible to investigate and characterize them by vibrational and electronic spectroscopy. Solutions of the monooxidized forms are sufficiently long-lived that these systems are viable synthetic targets. Further studies that aim at their isolation and a more comprehensive assessment of their electronic and magnetic properties are currently underway in our laboratories.

Acknowledgment. Support of this work by the Deutsche Forschungsgemeinschaft (Grants Wi 1262/7-1 and 436 TSE 113/45/0-1), the EU (COST actions D35), and the Grant Agency of the Academy of Sciences of the Czech Republic (S.Z., Grant 1ET400400413) is gratefully acknowledged. We also acknowledge contributions from Barbara Vogel during an advanced course in our laboratories.

Supporting Information Available: One-electron energies and percentage compositions of selected orbitals of **p-2^{Me}** and **m-2^{Me}** (Tables S1 and S2), symmetry-averaged bond lengths and angles for **p-2^{Me}** and **m-2^{Me}** in their various oxidation states (Tables S3 and S4), lowest calculated excitation energies for **p-2^{Me}** and **m-2^{Me}** as calculated by TDDFT (Tables S5 and S6), the ESR spectrum of **m-2^{Me+}** (Figure S1) and the UV/vis/near-IR and IR spectra of **p-2^{Me+}** and **m-2^{Me+}** generated by bulk electrolysis (Figures S2 and S3), charge density difference plots for the first oxidations of **p-2^{Me}** and **m-2^{Me}** (Figure S4), calculated atomic displacements for the C═C stretch/CH bend of **p-2^{Me}** (Figure S5), and IR spectroelectrochemistry for further oxidation of **m-2**$^+$ to **m-2**$^{2+}$ on a larger energy scale (Figure S6). This material is available free of charge via the Internet at http://pubs.acs.org.

OM0602660

(92) Brunschwig, B.; Creutz, C.; Sutin, N. *Chem. Soc. Rev.* **2002**, *31*, 168.